Receptor Binding Kinetics and Cellular Responses of Six N-Formyl Peptide Agonists in Human Neutrophils†

Anna Waller,‡ Karyn L. Sutton,⊗,‡,§, Tamara L. Kinzer-Ursem,⊗,‡ Afaf Absood,§ John R. Traynor,|| Jennifer J. Linderman,‡ and Geneva M. Omann*,§,⊥,#

Departments of Chemical Engineering, Surgery, Pharmacology, and Biological Chemistry, University of Michigan, and VA Medical Center, Ann Arbor, Michigan 48105

Received July 28, 2003; Revised Manuscript Received April 21, 2004

ABSTRACT: The goal of this study was to elucidate the relationships between early ligand binding/receptor processing events and cellular responses for the N-formyl peptide receptor system on human neutrophils as a model of a GPCR system in a physiologically relevant context. Binding kinetics of N-formyl-methionyl-leucyl-phenylalanyl-phenylalanyl-lysine-fluorescein and N-formyl-valyl-leucyl-phenylalanyl-lysine-fluorescein to the N-formyl peptide receptor on human neutrophils were characterized and combined with previously published binding data for four other ligands. Binding was best fit by an interconverting two-receptor state model that included a low affinity receptor state that converted to a high affinity state. Response behaviors elicited at 37 °C by the six different agonists for the N-formyl peptide receptor were measured. Dose response curves for oxidant production, actin polymerization, and G-protein activation were obtained for each ligand; whereas all ligands showed equal efficacy for all three responses, the ED_{50} values varied as much as 7000-fold. The level of agonism and rank order of potencies of ligands for actin and oxidant responses were the same as for the G-protein activation assay, suggesting that the differences in abilities of ligands to mediate responses were determined upstream of G-protein activation at the level of ligand−receptor interactions. The rate constants governing ligand binding and receptor affinity conversion were ligand-dependent. Analysis of the forward and reverse rate constants governing binding to the proposed signaling receptor state showed that it was of a similar energy for all six ligands, suggesting the hypothesis that ligand efficacy is dictated by the energy state of this ligand−receptor complex. However, the interconverting two-receptor state model was not sufficient to predict response potency, suggesting the presence of receptor states not discriminated by the binding data.

Understanding the relationship between ligand binding and response generation for GPCRs[1] is complicated by a number of dynamic events that occur at the level of the receptor. Receptors may exist in active and inactive states (*1*−*5*). Binding of ligand to the receptor may activate G-proteins, cause a change in affinity for ligand, and induce receptor phosphorylation and arrestin binding (*6*−*11*). Ligand−receptor complexes may be internalized and recycled to the cell surface (*12*−*15*). Uncovering the roles that each of these events play in response generation requires studies that focus on the different temporal aspects of ligand binding, receptor processing, and response generation.

Much of what is known about GPCRs has been obtained from purified receptors reconstituted into membranes and mutationally manipulated receptors expressed in model tissue culture cell systems (*1*, *5*, *7*, *10*, *16*−*19*). Whereas these approaches have revealed much about the physical properties of receptors and the nature of the molecules involved in GPCR signaling, they are not well suited to determine how the early temporal characteristics of ligand/receptor binding and processing relate to physiologically relevant responses.

The N-formyl peptide receptor on neutrophils is an excellent system in which to study the roles that the early (sec-min) receptor-level events play in response generation in a GPCR system. The N-formyl peptide receptor recognizes bacterial N-formyl peptides and couples with G_i proteins to elicit inflammatory responses that include chemotaxis, oxidant production, and degranulation (*20*). A particular advantage to this system is that the dynamics of receptor/

† This work was supported by the National Science Foundation BES-9713956; National Institutes of Health #DA04087 and #GM62930; Office of Research and Development, Medical Research Service, Department of Veterans Affairs; the Alfred P Sloan Foundation; and the GE Foundation.

* To whom correspondence should be addressed. Geneva M. Omann, Ph.D., Research Service (11R), VA Medical Center, 2215 Fuller Road, Ann Arbor, MI 48105. Tel.: 734-769-7100 ex 5238. Fax: 734-761-7693. E-mail: gmomann@umich.edu.

‡ Department of Chemical Engineering University of Michigan.

§ Department of Surgery University of Michigan.

|| Department of Pharmacology University of Michigan.

⊥ Department of Biological Chemistry University of Michigan.

VA Medical Center.

⊗ These authors contributed equally to this work.

[1] Abbreviations: BSA, bovine serum albumin; CHO-NLFNYK-FL, N-formyl-norleucyl-leucyl-phenylalanyl-norleucyl-tyrosyl-lysine-fluorescein; CHO-NLFNYK-TMR, N-formyl-norleucyl-leucyl-phenylalanyl-norleucyl-tyrosyl-lysine-tetramethyrhodamine; CHO-NLF, N-formyl-norleucyl-leucyl-phenylalanine; CHO-MLF, N-formyl-methionyl-leucyl-phenylalanine; CHO-MLFFK-FL, N-formyl-methionyl-leucyl-phenylalanyl-phenylalanyl-lysine-fluorescein, CHO-VLFK-FL, N-formyl-valyl-leucyl-phenylalanyl-lysine-fluorescein; DMSO, dimethyl sulfoxide; GPCR, G-protein coupled receptor; HSB, buffer containing 5 mM KCl, 147 mM NaCl, 1.9 mM KH_2PO_4, 0.22 mM Na_2HPO_4, 5.5 mM glucose, 0.3 mM $MgSO_4$, 1 mM $MgCl_2$, and 10 mM HEPES, at pH 7.4.

10.1021/bi035335i CCC: $27.50
Published on Web 06/04/2004

ligand binding has been carefully characterized using fluorescently labeled ligands and real time, flow cytometric methods (*21*, *22*). Recent studies have identified both an early, low affinity ligand-bound receptor state and a later, high affinity ligand-bound state (*21*−*24*). In addition, the G_i-linked actin polymerization and oxidant production of single cells can be measured in real time with high kinetic resolution (*25*−*28*). While the time scales of actin polymerization and oxidant production differ, they are both relatively short when compared with the time for ligand binding to reach equilibrium (*22*, *27*−*29*). Therefore, ligand−receptor binding and processing kinetic parameters, and not equilibrium constants, are likely to be the relevant parameters in controlling these particular cellular responses (*22*, *30*). Thus, the N-formyl peptide receptor system is uniquely suited to address the question of how the identified receptor states and their kinetics of formation relate to cellular responses.

To adequately address this question, one needs a group of ligands that possess different receptor−ligand binding and processing kinetics and for which responses can be measured. Short N-formyl peptide sequences that bind to the N-formyl peptide receptor with a range of affinities can be readily made and fluorescently labeled (*31*−*33*). In the pioneering flow cytometric studies of Sklar and co-workers (*21*) and more recently in the high time resolution flow cytometric studies of Hoffman et al. (*23*) and Waller et al. (*24*), it has been demonstrated that the binding of four N-formyl peptides, CHO-NLFNYK-FL, CHO-NLFNYK-TMR, CHO-NLF, and CHO-MLF, at 4 °C can be described by a two-site, interconverting receptor binding scheme:

Scheme 1

$$L + R_s \underset{k_f}{\overset{k_r}{\leftrightarrows}} LR_s \xrightarrow{k_x} LR_x \underset{k_{r2}}{\overset{k_{f2}}{\leftrightarrows}} L + R_x$$

In this scheme, ligand (L) binds to surface receptors (R_s) with rate constant k_f to form low-affinity receptor−ligand complexes (LR_s), which convert to high-affinity complexes (LR_x) with rate constant k_x. High-affinity complexes are also formed by ligand binding to high-affinity state receptors (R_x) with the rate constant k_{f2}. Ligand can dissociate from low- or high-affinity receptor−ligand complexes with rate constants k_r and k_{r2}, respectively. At 4 °C, receptor trafficking is minimized, and the total number of surface receptors, R_{tot}, equal to the sum of the receptor states described above, remains constant. Significantly, key rate constants, including k_f, k_r, and k_x, of Scheme 1 were found to be ligand-dependent. As reported previously (*29*, *34*, *35*), the low-affinity receptor−ligand complex is believed to be the receptor state responsible for signaling. Thus the rate constants k_f, k_r, and k_x, which govern the formation and lifetime of the low-affinity receptor−ligand complex, may be critical for determining cellular response characteristics.

In this manuscript, we first enlarge our pool of ligands for which kinetics have been measured by determining the binding kinetics for two additional N-formyl peptide ligands, CHO-MLFFK-FL and CHO-VLFK-FL, in an attempt to expand the range of binding properties studied and determine the wider applicability of Scheme 1. Previously reported results indicate that CHO-MLFFK-FL is a more potent ligand than CHO-NLFNYK-FL (*31*, *32*, *36*), the most potent of the four listed above, and thus CHO-MLFFK-FL has the potential of exhibiting faster ligand binding kinetics or slower rate of conversion to the LR_x state than CHO-NLFNYK-FL. There are no previously published data regarding the binding or response characteristics of CHO-VLFK-FL; however, studies of N-formyl peptides with valyl in the first position suggest it would be a relatively weak agonist (*37*).

In addition, we collect actin polymerization and oxidant production response data for all 6 ligands. We also use an assay for G-protein activation to demonstrate that the ligand specific differences in responses are likely determined upstream of G-protein activation (i.e., at the level of the receptor−ligand binding kinetics we have measured). Finally, with both the relevant kinetic binding data (rate constants of Scheme 1) and the response data for all six ligands in hand, we then examine the data for relationships between the measured rate constants and responses. We note a relationship between the energy state of the low affinity receptor state and ligand efficacy, and we examine the hypothesis that the number of low affinity ligand-bound receptors in this system is a predictor of the cellular potency.

MATERIAL AND METHODS

Reagents. Standard cellular and ligand buffer, HSB, contained 5 mM KCl, 147 mM NaCl, 1.9 mM KH_2PO_4, 0.22 mM Na_2HPO_4, 5.5 mM glucose, 0.3 mM $MgSO_4$, 1 mM $MgCl_2$, and 10 mM HEPES, at pH 7.4. [^{35}S]GTγS was obtained from Perkin-Elmer Life Sciences (Boston, MA). 50× protease inhibitor cocktail was obtained from BD Biosciences (San Diego, CA). DMSO was purchased from Pierce Chemical Co. (Rockford, IL). The peptide WKYMVM-NH_2 was synthesized by the Peptide Synthesis Facility of the University of Michigan. CHO-NLFNYK-FL and CHO-NLFNYK-TMR were obtained from Molecular Probes, Inc (Eugene, OR). All other reagents were purchased from Sigma Chemical Company (St. Louis, MO) and were of analytical grade. Ligands were stored in stock solutions of 10^{-3} M in DMSO. For each experiment, an aliquot of ligand in DMSO was diluted into HSB with 0.1% BSA to give solutions 100-fold more concentrated than those required for the experiment. BSA was included to minimize nonspecific binding of ligand to vial surfaces. Final 1 to 100 dilutions of ligands were made into the cell suspensions for either binding or response assays.

Neutrophil Isolation and Preparation of Plasma Membranes. Neutrophils were isolated via the protocol of Tolley et al. (*38*). Isolated neutrophils were stored at 4 °C in HSB buffer at 10^8 cells/mL prior to use (within 1 h).

To isolate plasma membranes, neutrophils were resuspended in buffer containing 10 mM HEPES, 0.1 M sucrose, 1 mM EGTA, 1/50 dilution of 50× protease inhibitor cocktail, pH 7.3 and nitrogen cavitated at 450 psi for 15 min at 4 °C (*39*). The cavitate was centrifuged for 10 min at 4 °C and 500*g* to remove intact cells and nuclei. This supernatant was centrifuged for 15 min at 4 °C and 8000*g* to remove granules. Finally, the supernatant was centrifuged for 30 min at 4 °C and 200000*g*. The pellet containing the plasma membranes was homogenized with 1 mL of 50 mM Tris-HCl buffer (pH 7.4) and aliquoted for storage at −70 °C. Protein quantitation was performed by the Bradford method using the Coomassie Protein Assay Reagent (Pierce, Rockford, IL) with BSA as a standard (*40*).

Synthesis and Purification of Fluorescein-Labeled Pentapeptide and Tetrapeptide. The pentapeptide CHO-MLFFK-FL was synthesized, purified, and characterized as previously described (*24*). The tetrapeptide, CHO-VLFK, was synthesized by the Peptide Synthesis Facility of the University of Michigan and was fluorescein-labeled using procedures similar to that for the labeling of CHO-MLFFK except that fluorescein succinimidyl ester (Molecular Probes, Inc. Eugene, OR) was used instead of fluorescein isothiocyanate. Thin layer chromatographic purification of CHO-VLFK-FL was analogous to that described for CHO-MLFFK-FL (*24*), using a solvent system of chloroform/methanol/acetic acid (3:1:0.01; v/v/v) (*41*, *42*).

Equilibrium Binding Assay for Fluorescently Labeled Ligands. The total number of N-formyl peptide receptors on the cell surface was measured using a 4 °C equilibrium binding assay described by Sklar and Finney (*43*) and detailed in Waller et al. (*24*). Concentration ranges utilized were 0.1−3 nM for CHO-NLFNYK-FL, 0.025−1 nM for CHO-MLFFK-FL, and 0.1−40 nM for CHO-VLFK-FL. In all binding studies, CHO-NLFNYK-FL binding was also characterized to confirm agreement with previously published data (*23*, *24*). Fluorescence bound to cells was measured by flow cytometry and quantified as fluorescence mean channel number. After subtraction of nonspecific binding, the specifically bound fluorescence was converted to ligand bound per cell using a standard curve of fluorescein-labeled standard beads and the calibration values, Q, equal to 1.02 and 0.83 for CHO-NLFNYK-FL and CHO-MLFFK-FL, respectively, as described (*24*). The calibration value Q was found to be 0.83 for CHO-VLFK-FL by comparison of equilibrium binding curves with those of CHO-NLFNYK-FL as described (*24*).

The bound receptor data (i.e., the number of receptor−ligand complexes) were described by a one-site model

$$[\mathrm{LR}] = \frac{R_{\mathrm{tot}}[\mathrm{L}]}{[\mathrm{L}] + K_{\mathrm{dapp}}} \quad (1)$$

where [L] is the ligand concentration, and [LR] is the concentration of specifically bound receptors per cell. The total number of surface N-formyl peptide receptors, R_{tot}, and the apparent equilibrium dissociation constant, K_{dapp}, were evaluated by minimizing the squared residual of the data points and model by nonlinear regression in Microsoft Excel. Incubations of 1 and 12 h did not yield significantly different estimates for either R_{tot} or K_{dapp} for CHO-NLFNYK-FL and CHO-MLFFK-FL, confirming that equilibrium was reached within 1 h (data not shown). Thus, samples for the equilibrium curves were allowed to incubate for 1−2 h before measuring binding. R_{tot} calculated from these curves indicated the number of surface receptors available for binding ligand. The significance of K_{dapp} calculated for each ligand will be discussed below.

Kinetic Binding Assays. An association protocol (Protocol A) and dissociation protocol (Protocol B) were used to monitor the kinetic binding of CHO-MLFFK-FL and CHO-VLFK-FL, as previously detailed for CHO-NLFNYK-FL (*23*, *24*). For the association Protocol A, binding of fluorescently labeled ligand to cells (1×10^6 cells/mL) was measured after a bolus addition of fluorescently labeled ligand. For the dissociation Protocol B, fluorescently labeled ligand was allowed to bind to cells for various periods of time, and then a large excess of unlabeled ligand (3×10^{-5} M CHO-MLF) was added and dissociation of fluorescent ligand measured. Dissociation was initiated at different time scales, after a short time (15−90 s of binding), or after a long time (more than 2 h of binding), to capture the different receptor affinity states. Samples were maintained at 4 °C throughout the duration of the assay.

Analysis of Kinetic Binding Data. For each kinetic data set, nonspecific binding was subtracted and fluorescence mean channel number converted to ligand bound per cell, as described for equilibrium binding data. Kinetic binding data for CHO-MLFFK-FL were analyzed as previously described for CHO-NLFNYK-FL (*23*, *24*). Long time (after 1−2 h of binding) dissociation data were best fit to a single-exponential decay, indicating that the receptors had been converted to the high affinity state. The decay constant obtained from these data was thus k_{r2}. k_{r2} and K_{dapp} calculated from the equilibrium binding curve were used to calculate $k_{f2} = k_{r2}/K_{\mathrm{dapp}}$, with the assumption that $K_{\mathrm{dapp}} = K_{\mathrm{dx}}$. k_f, k_r and k_x were determined by fitting association data and short-time dissociation data with the interconverting two-site binding model (Scheme 1) using MicroMath Scientist software (MicroMath Scientific Software, Salt Lake City, UT) while holding the values of k_{f2} and k_{r2} constant at the values determined from the long-term dissociation. Validation of the assumptions that K_{dapp} determined from the equilibrium binding curve and k_{r2} determined from long-time dissociation data reflect characteristics of the high affinity receptor state, R_x, is given in Results. CHO-MLFFK-FL concentrations of 1 and 3 nM were utilized to validate that the values of the rate constants were independent of ligand concentration.

Data analyses of CHO-VLFK-FL binding were made with modified analysis protocols necessitated by the observation of two receptor states during the long-time dissociation protocol that indicated the value for the conversion rate constant, k_x, was small compared with the other fluorescently labeled ligands studied. In this case, the assumption that K_{dapp} from equilibrium binding curves (after 1−2 h of binding) was equivalent to K_{dx} was not valid. Thus, the association binding data from Protocol A for CHO-VLFK-FL were fit to the interconverting two-site binding model (Scheme 1) using MicroMath Scientist software, while varying all rate constants: k_f, k_r, k_x, k_{r2}, and k_{f2}. The values calculated for k_{r2} and k_{f2} from association binding data did not pass the confidence criteria ratio (that the standard deviation determined by the software was less than 1/10 of the value of the rate constant). However, this analysis yielded statistically significant estimates for k_f and k_r. Next, the short-time and long-time dissociation data from Protocol B were fit to the complete two-site binding model with k_f constrained to the value calculated from association data. Furthermore, due to the significant presence of both LR_s and LR_x at the time of collecting long-time dissociation data, these data needed to be analyzed with the initial conditions set such that zero time was the time at which fluorescently labeled ligand was added (LR_s and LR_x equaled zero). The dissociation binding data thus analyzed yielded greater confidence in the later reaction rate constants, k_r, k_x, k_{r2}, and k_{f2}. An alternative data analysis scheme was utilized to validate this approach, as described in the Appendix.

Response Assays. Three responses were monitored in this study, one proximal and two distal to ligand−receptor binding. G-protein activation was measured as the first step in the signal transduction cascade after ligand−receptor binding. Actin polymerization and oxidant production were monitored as downstream responses mediated by signaling pathways that diverge after G-protein activation. Actin polymerization is a rapid (seconds) response that does not require calcium mobilization. The oxidant response develops over minutes and is a calcium-dependent pathway.

Actin Polymerization Assay. Dynamic actin polymerization was monitored by right angle light scattering on a spectrofluorometer (SLM-Aminco 8100, Urbana, IL) as described (*27*). Cell solutions of 2×10^6 cells/mL HSB plus 1.5 mM Ca^{2+} were incubated at 37 °C about 10 min prior to assay. A baseline of cellular right angle light scatter at 340 nm was collected in a continuously stirred cuvette for the initial 20 s, at which time a bolus of stimulating ligand was added and the response monitored for an additional 80 s. Under these conditions, the right angle light scatter signal is inversely related to the F-actin content (*27*). Responses were measured over a range of ligand concentrations and quantified both as the maximum magnitude of change in right angle light scatter and the maximum rate of change in right angle light scatter. Because there was day-to-day variability in the maximum magnitude of change (likely due to donor variability), data from a particular day was normalized to the maximum magnitude of response of CHO-NLFNYK-FL on that day. The rate of change of right angle light scatter seemed less sensitive to donor variability, thus it was quantified as fractional change per second. The concentrations of ligands that gave 50% maximal responses (ED_{50}) were determined from fits of the data to a sigmoidal function using Prism GraphPad software (San Diego, CA).

Oxidant Assay. Oxidant production was measured spectrofluorometrically based on protocols described by Hyslop and Sklar (*28*). Neutrophils at 2×10^6 cells/mL HSB plus 1.5 mM Ca^{2+} were incubated at 37 °C for 10 min, and then a 100-fold concentrated cocktail was added to give final concentrations of 10 μg/mL para-hydroxyphenylacetic acid, 8 μg/mL superoxide dismutase, and 8 μg/mL horseradish peroxidase. Ligand was added and the fluorescence monitored on a spectrofluorometer (SLM-Aminco 8100, Urbana, IL) with excitation wavelength of 323 nm and emission wavelength of 400 nm. In this assay, superoxide dismutase converts O_2^- into H_2O_2, which reacts with peroxidase and para-hydroxyphenylacetic acid to produce a fluorescent diadduct. The fluorescence was calibrated with known amounts of H_2O_2 solution. Oxidant production was monitored with the use of a four-sample rotating turret, which allowed collection of one data point every 4 s for each of four samples. Responses were measured over a range of ligand concentrations and quantified both as the total amount of oxidants produced and the maximum rate of oxidant production. Because there was some variability in the magnitude and rate of response from day to day, data from a particular day was normalized to the maximum response (magnitude and rate) of CHO-NLFNYK-FL on that day. The concentrations of ligands that gave 50% maximal responses (ED_{50}) were determined from fits of the data to a sigmoidal function using Prism GraphPad software (San Diego, CA).

[^{35}S]GTPγS Binding Assay. Activation of G-proteins was assayed by measuring the binding of [^{35}S]GTPγS to neutrophil plasma membranes following the protocol most recently outlined by Clark et al. (*44*). Neutrophil plasma membranes (3−5 μg protein) were incubated in the presence of 20 mM Tris-HCl (pH 7.4), 100 mM NaCl, 5 mM $MgCl_2$, 1mM EDTA, 1mM dithiothreitol (added fresh), 100 μM GDP, 0.1 nM [^{35}S]GTPγS, and varying concentrations of ligand or vehicle (HSB buffer plus 0.1% BSA) in a total volume of 200 μL at 25 °C. Binding over a 1 h time period was linear, thus the incubation time was set at 1 h. Bound and free [^{35}S]GTPγS were separated by vacuum filtration through glass-fiber filters (No. 32, Schleicher and Shuell) in a Brandel cell harvester. Membranes were rinsed four times with ice-cold 50 mM Tris-HCl, pH 7.4, 5 mM $MgCl_2$, and 100 mM NaCl. Radioactivity retained on the filters was counted by liquid scintillation counting in 4 mL of EcoLume scintillation cocktail (INC, Aurora, OH). [^{35}S]GTPγS bound to membranes was measured over a range of ligand concentrations and reported as percent above basal [^{35}S]GTPγS binding. The maximal amount of [^{35}S]GTPγS binding and the concentration of ligand that gave 50% maximal response (ED_{50}) were determined from fits of the data to a sigmoidal function using Prism software (GraphPad Software, Inc., San Diego, CA).

Linear Correlation Analyses of Parameters. To determine if there were linear relationships among the parameters measured, the data of Table 1 were analyzed by generating a correlation matrix using Instat software (GraphPad Software, Inc.). This analysis evaluated pairs of parameters across all six ligands to determine if linear relationships existed. The degree of correlation was given as the correlation coefficient, *r*, as reported in Table 2. For some combinations of parameters, multiple regression analyses were performed using GraphPad Instat software.

Relationships between Ligand−Receptor Complexes and Responses. To test for the ability of Scheme 1 to predict response potency, the equations describing the model (*22*) were utilized to calculate the rate of formation and amount of LR_s and LR_x for each experimental concentration of each ligand. For these calculations, the rate constants measured at 4 °C were converted to their 37 °C equivalents using an Arrhenius conversion factor of 8 kcal/mol (*23*, *51*); measurement of CHO-NLFNYK-FL binding kinetics at both 4 °C and 37 °C confirm that this conversion is valid (*23*). Receptor internalization, which affects the number of LR_x but not LR_s, is negligible over the short time during which responses are generated (*51*). Simulations of LR_s and LR_x formation were performed for each ligand concentration using Mathematica (Wolfram Research, Champaign, IL) and from these data the rate of complex formation and the amount of complex integrated over time (10 s for actin response and 300 s for oxidant response) were calculated. "Dose−response" curves were then generated for measured responses versus calculated rate or amount of ligand−receptor complex formation and the data fit to a sigmoidal function using Prism GraphPad software (San Diego, CA). To account for uncertainties in values of the rate constants, predictions were also made for two limiting cases, high ligand−receptor complex and low ligand−receptor complex. For example, the rate constants that govern the magnitude of LR_s are k_f, k_r, and k_x. Therefore, the prediction for the high LR_s case was made with a large

Table 1: Binding Constants and Responses of Six N-formyl Peptides

ligand[a]	CHO-MLFFK-FL	CHO-NLFNYK-FL	CHO-NLFNYK-TMR	CHO-VLFK-FL	CHO-MLF	CHO-NLF
			binding constants[e]			
k_f (M^{-1} s^{-1})	**$8.6 \pm 0.8 \times 10^6$ (13)**[b]	*7.4* $\pm$ 0.5 $\times$ 10^6 (16)[c]	*3.1* $\pm$ 0.2 $\times$ 10^6 (16)[c]	**$4.1 \pm 1.2 \times 10^6$ (5)**	*1.2* $\pm$ 0.4 $\times$ 10^7 (6)[d]	*4.0* $\pm$ 1.5 $\times$ 10^7 (3)[d]
k_r (s^{-1})	**$4.8 \pm 0.4 \times 10^{-2}$ (13)**	*1.1* $\pm$ 0.06 $\times$ 10^{-1} (16)	*1.2* $\pm$ 0.05 $\times$ 10^{-1} (16)	**$7.8 \pm 2.0 \times 10^{-2}$ (6)**	*5.5* $\pm$ 1.4 $\times$ 10^{-1} (6)	*2.4* $\pm$ 0.6 (3)
k_x (s^{-1})	**$1.6 \pm 0.1 \times 10^{-2}$ (13)**	*2.4* $\pm$ 0.1 $\times$ 10^{-2} (16)	*1.5* $\pm$ 0.09 $\times$ 10^{-2} (16)	**$1.8 \pm 0.7 \times 10^{-4}$ (6)**	*1.1* $\pm$ 0.1 $\times$ 10^{-4} (3)	*1.0* $\pm$ 0.4 $\times$ 10^{-4} (2)
k_{r2} (s^{-1})	**$6.4 \pm 0.9 \times 10^{-4}$ (13)**	*9.3* $\pm$ 1.0 $\times$ 10^{-4} (16)	*1.3* $\pm$ 0.08 $\times$ 10^{-3} (16)	**$1.5 \pm 0.5 \times 10^{-3}$ (5)**	*1.6* $\pm$ 0.3 $\times$ 10^{-5} (2)	*1.3* $\pm$ 0.3 $\times$ 10^{-5} (2)
k_{f2} (M^{-1} s^{-1})	**$1.5 \pm 0.2 \times 10^7$ (13)**	*2.1* $\pm$ 0.2 $\times$ 10^6 (16)	*6.2* $\pm$ 0.5 $\times$ 10^5 (16)	**$2.3 \pm 1.0 \times 10^6$ (5)**	4.7 $\times$ 10^2 (2)	4.3 $\times$ 10^1 (2)
K_{ds} (M)[f]	**5.6×10^{-9}**	1.5 $\times$ 10^{-8}	4 $\times$ 10^{-8}	**1.9×10^{-8}**	4.6 $\times$ 10^{-8}	6.0 $\times$ 10^{-8}
K_{dx} (M)[g]	**4.4×10^{-11}**	4.4 $\times$ 10^{-10}	2.0 $\times$ 10^{-9}	**6.6×10^{-10}**	3.4 $\times$ 10^{-8}	3.0 $\times$ 10^{-7}
			responses (ED_{50}, M)[h]			
actin rate	**2×10^{-11}**	**5×10^{-11}**	**2×10^{-10}**	**1×10^{-10}**	**1×10^{-9}**	**2×10^{-9}**
actin magnitude	**3×10^{-12}**	**9×10^{-12}**	**4×10^{-11}**	**1×10^{-10}**	**1×10^{-9}**	**2×10^{-9}**
oxidant rate	**1×10^{-11}**	**2×10^{-10}**	**1×10^{-9}**	**3×10^{-9}**	**5×10^{-8}**	**8×10^{-8}**
oxidant magnitude	**2×10^{-11}**	**2×10^{-10}**	**1×10^{-9}**	**4×10^{-9}**	**3×10^{-8}**	**2×10^{-7}**
[^{35}S]GTPγS binding	**4×10^{-9}**	**2×10^{-9}**	**8×10^{-9}**	**1×10^{-7}**	**2×10^{-7}**	**1×10^{-6}**

[a] Ligands are listed by order of response ED_{50} values from lowest to highest. [b] Values in bold type were determined in this work. Values in italics were taken from previously published work, as indicated. [c] Binding constants reported by Waller et al. (*24*). [d] Binding constants reported by Hoffman et al. (*23*). [e] Mean $\pm$ SEM, *n* in parentheses. [f] Calculated as k_r/k_f. [g] Determined from equilibrium binding curves, K_{dapp}, or as k_{r2}/k_{f2}. [h] Response ED_{50} values determined in this work. Estimated error is $\pm$ 50%.

Table 2: Correlation Matrix for Binding Constants and Responses[a]

	k_f	k_r	k_x	k_{r2}	k_{f2}	K_{ds}	K_{dx}	AR	AM	OR	OM	GTP
k_f	**1.0**											
k_r	**0.986**	**1.0**										
k_x	−0.452	−0.518	**1.0**									
k_{r2}	−0.730	−0.678	0.356	**1.0**								
k_{f2}	−0.237	−0.366	0.380	0.062	**1.0**							
K_{ds}	0.682	0.777	−0.594	−0.553	−0.717	**1.0**						
K_{dx}	**0.986**	**0.996**	−0.484	−0.630	−0.322	0.734	**1.0**					
AR[b]	**0.934**	**0.961**	−0.632	−0.781	−0.455	0.871	**0.932**	**1.0**				
AM	**0.938**	**0.958**	−0.652	−0.796	−0.429	0.841	**0.928**	**0.997**	**1.0**			
OR	**0.898**	**0.918**	−0.671	−0.835	−0.441	0.847	**0.879**	**0.989**	**0.993**	**1.0**		
OM	**0.987**	**0.998**	−0.512	−0.645	−0.355	0.747	**0.999**	**0.943**	**0.941**	**0.900**	**1.0**	
GTP	**0.978**	**0.994**	−0.577	−0.635	−0.361	0.754	**0.997**	**0.950**	**0.950**	**0.908**	**0.997**	**1.0**

[a] Correlations are given as the correlation coefficient, *r*. Those correlations that are high, greater than approximately 0.900, are shown in bold type. [b] AR, rate of actin polymerization; AM, magnitude of actin polymerization; OR, rate of oxidant production; OM, magnitude of oxidant production; GTP, [^{35} S] GTPγS.

value of k_f (mean value plus one standard error of the mean) and small values for k_r and k_x (mean value minus one standard error of the mean). Conversely, the simulation for the low LR_s case was made with large values of k_r and k_x (mean value plus one standard error of the mean) and small values of k_f (mean value minus one standard error of the mean).

RESULTS

Characterization of N-Formyl Peptide Binding Behavior.

Equilibrium Binding of CHO-MLFFK-FL and CHO-VLFK-FL. The apparent equilibrium constants, K_{dapp}, for CHO-MLFFK-FL and CHO-VLFK-FL were found to be 0.04 nM and 4.6 nM, respectively. Consistent with literature reports (*23*, *24*) a K_{dapp} value of 0.4 nM was obtained for CHO-NLFNYK-FL. Nonspecific binding for CHO-NLFNYK-FL and CHO-MLFFK-FL was shown to be linear; however, for CHO-VLFK-FL, nonspecific binding diverged from a linear fit at concentrations above 15 nM. The reason for this deviation has not been resolved, but light scattering measurements showed it could not be attributed to precipitation of ligand. At lower ligand concentrations (<15 nM), the magnitude of nonspecific binding for CHO-VLFK-FL corresponded with the magnitude of nonspecific binding of the other ligands. Any difficulty in correcting for nonspecific binding of CHO-VLFK-FL was avoided in our equilibrium and kinetic binding experiments by using concentrations that did not exceed 10 nM.

Kinetic Binding of CHO-MLFFK-FL and CHO-VLFK-FL. The kinetics of ligand association were monitored via protocol A, as shown in Figure 1 for CHO-MLFFK-FL and CHO-VLFK-FL. The kinetics of ligand dissociation were monitored following either a short (15−90 s) or a long (hours) period of ligand binding (Protocol B). Ligand dissociation was initiated by adding CHO-MLF at a 1000-fold greater concentration than labeled ligand. Figure 2 depicts dissociation of CHO-MLFFK-FL and CHO-VLFK-FL following a long period of binding. For CHO-MLFFK-FL, labeled ligand dissociation was slow, as observed by the small decrease in the number of bound receptors per cell after addition of CHO-MLF (Figure 2A). Furthermore, dissociation data collected after even longer periods of ligand binding (e.g., 3.5 h) showed evidence of the same slow dissociation rate. This type of dissociation is indicative of the presence of a single receptor state, and these data were best fit using a single-exponential decay model to yield k_{r2}. Thus, for CHO-MLFFK-FL (as has been observed with CHO-NLFNYK-FL), only one receptor state was present after 2 h of binding, which was the same time scale for collecting equilibrium binding data. Therefore, it was assumed that the K_{dapp} calculated from equilibrium binding data

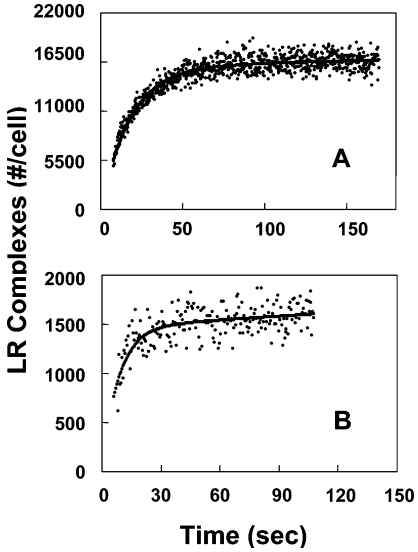

FIGURE 1: Association binding of fluorescently labeled ligands. Kinetic binding data (dots) and model fits (lines) are shown for ligand binding to the N-formyl peptide receptor collected via Protocol A. (A) 3 nM CHO-MLFFK-FL and (B) 3 nM CHO-VLFK-FL. These data were collected on different days, and thus R_{tot} differed for each panel.

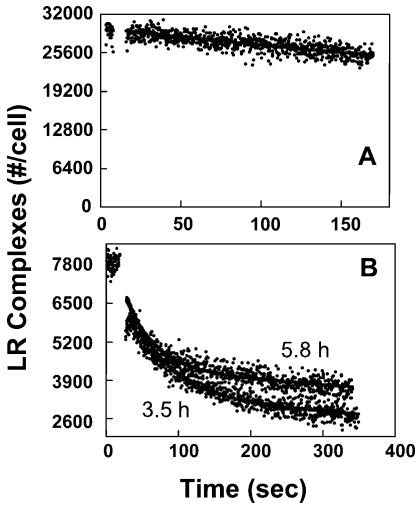

FIGURE 2: Long-time dissociation measurements of fluorescently labeled ligands. Dissociation data (dots) and model fits (lines) are shown for ligand bound to the N-formyl peptide receptor. (A) Dissociation was initiated by addition of CHO-MLF after 2 h of binding of 1 nM CHO-MLFFK-FL. (B) Dissociation was initiated by addition of CHO-MLF after 3.5 and 5.8 h of binding by 3 nM CHO-VLFK-FL. These data were collected on different days, and thus R_{tot} differed for each panel.

was equal to K_{dx} and was utilized to calculate k_{f2}, ($K_{dapp} = K_{dx} = k_{r2}/k_{f2}$).

The dissociation of CHO-VLFK-FL following a long period of binding is shown in Figure 2B. The dissociation of the labeled ligand showed an initial rapid phase of about 10−15 s and then a slower phase with dissociation kinetics more similar to that observed in Figure 2A for CHO-MLFFK-FL. These data are indicative of receptors present in more than one affinity state. The initial rapid dissociation is attributed to the presence of LR_s, the low-affinity receptor−ligand complex, while the gradual fluorescence decrease is due to the slower dissociation of the ligand from the higher affinity receptor state, LR_x. The implication of the appearance of different receptor states after this long-time binding period

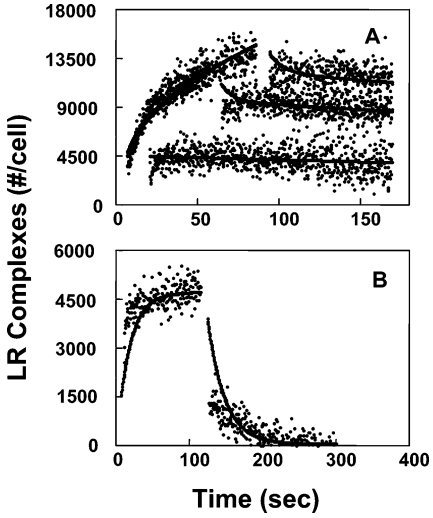

FIGURE 3: Short-time dissociation measurements of fluorescently labeled ligands. Short-time dissociation data (dots) and model fits (lines) are plotted for ligand bound to the N-formyl peptide receptor: (A) dissociation of 1 nM CHO-MLFFK-FL initiated after 15, 60, and 90 s of binding. (B) dissociation of 10 nM CHO-VLFK-FL initiated after 2 min of binding. These data were collected on different days, and thus R_{tot} differed for each panel.

is that the receptor state interconversion rate constant, k_x, is small. Thus, the K_{dapp} reported above calculated with the equilibrium binding protocol for CHO-VLFK-FL represented a combination of the different receptor affinity states. Collection of dissociation data after several long-time intervals was made. Figure 2B shows long-time dissociation data of CHO-VLFK-FL that were initiated after 3.5 and 5.8 h of binding. Both dissociation curves show a rapid decrease in the number of bound receptors followed by a slower dissociation of ligand from receptor. However, the measured receptor−ligand affinity increased with longer times of ligand association, which agreed with the proposed interconverting two-site binding model.

To validate the existence of a low-affinity receptor−ligand complex that converts into a high-affinity receptor−ligand complex, short-time dissociation binding data were collected for CHO-MLFFK-FL and CHO-VLFK-FL (Figure 3). Figure 3A depicts the dissociation data for CHO-MLFFK-FL after binding for 15, 60, or 90 s. There was an initial rapid dissociation of the labeled ligand after the addition of CHO-MLF, which led into a second stage of more gradual dissociation, indicating the presence of two receptor states. Figure 3B shows dissociation of CHO-VLFK-FL after two minutes of binding, where the majority of the receptors were still in the more rapidly dissociating form.

The kinetic data were fit with the interconverting two-site binding model with the constraints detailed in Methods. For both ligands, the interconverting two-site binding model gave a statistically better fit than a one-site binding model when comparing the coefficient of determinants obtained from the data fits using the Scientist software (*23*, *24*). For example, the coefficient of determinants from association data of CHO-VLKF-FL fit to two-site binding model was 0.88 versus 0.63 for the same data fit to a one-site binding model. Thus, the published results for CHO-NLFNYK-FL, CHO-NLFNYK-TMR, CHO-MLF, and CHO-NLF (*23*, *24*) as well as the data presented here for CHO-VLFK-FL and CHO-MLFFK-FL support the interconverting two-site bind-

ing model of N-formyl peptide receptor binding and processing (Scheme 1).

The rate constants calculated from the kinetic data using the Scientist software and an interconverting two-site binding model at 4 °C for CHO-MLFFK-FL and CHO-VLFK-FL are listed in Table 1. Analysis of the table indicates that both ligands exhibit similar binding rate constants, with the exception of k_x, for which the CHO-VLFK-FL value is 2 orders of magnitude less than the CHO-MLFFK-FL value. Thus, the data clearly show that the rate of receptor interconversion is a ligand-dependent parameter.

Lack of N-Formyl Peptide Binding to FPRL-1. We note that the N-formyl peptide receptor has been cloned and homologues have been identified by low-stringency cross-hybridization with a cDNA from this clone (reviewed in ref *45*). One of these homologues, FPRL-1, is present in neutrophils and has been identified as the lipoxin A_4 receptor (*46*). Because of its low level of expression (~2000 receptors per cell) and low affinity for N-formyl peptides (*47*−*49*), it was not expected to contribute to binding measurements under the conditions of our experiments. However, experiments were designed to confirm this expectation. The hexapeptide WKYMVM-NH_2 has been shown to bind exclusively to FPRL-1, not the N-formyl peptide receptor, and induce calcium mobilization and oxidant production (*50*). If any of the N-formyl peptides utilized in our studies were capable of binding to FPRL-1, this binding would be competed off by WKYMVM-NH_2. Conversely, if the N-formyl peptides utilized in this study do not bind to FPRL-1, then the presence of WKYMVM-NH_2 in the binding assays would not affect the binding characteristics of the N-formyl peptides. Thus, equilibrium binding and kinetic assays were performed for two N-formyl peptides, CHO-NLFNYK-FL and CHO-VLFK-FL (that approximately span the range of potencies of the four fluorescent ligands) in the presence and absence of a saturating dose of WKYMVM-NH_2 (500 nM; *50*). The biological activity of WKYMVM-NH_2 was confirmed by performing oxidant and right angle light scatter assays. The ED_{50} for oxidant production was 50 nM, consistent with the value of 75 nM reported previously (*50*). The ED_{50} for the right angle light scatter response was 2 nM. The presence of 500 nM WKYMVM-NH_2 had no effect on the rate parameters determined for CHO-NLFNYK-FL or CHO-VLFK-FL, (compared with a two-tailed, paired t-test, $n = 4$, using GraphPad Instat software), indicating either that the N-formyl peptides did not bind to FPRL-1 or that FPRL-1 was present at such a low level that binding was insignificant compared to binding to N-formyl peptide receptor. In either case, the data confirmed that the rate parameters measured for N-formyl peptides reflected binding to only the N-formyl peptide receptor. Likewise, functional responses were a result of binding of the N-formyl peptides exclusively or predominantly to the N-formyl peptide receptor.

Interrelationships among Binding Parameters. Combined in Table 1 are the rate constants obtained in this study with those previously published for four other ligands. Data for the fluorescently labeled ligands CHO-NLFNYK-FL and CHO-NLFNYK-TMR were collected using methods identical to those used in this work, and thus we expect the published data and data reported in this work to be comparable. Although measurement of binding data for the unlabeled ligands, CHO-MLF and CHO-NLF, were collected by flow cytometric methods utilizing competitive binding protocols (*23*), we note that these competitive binding protocols have been independently validated (*24*). Thus, differences in binding characteristics between ligands cannot be attributed to differences in methodology.

Comparison of the rate constants governing formation of LR_s, the proposed signaling receptor state, showed that k_f varies over a 12-fold range, whereas k_r varies 50-fold among the six ligands. The K_{ds} values calculated from the rate constants are similar (less than 10-fold variation, compared with the 7000-fold variation in K_{dx} as discussed below), indicating that all the ligand−receptor complexes in the LR_s state have similar energies. The rate constants k_r and k_f are highly correlated (Table 2, $r = 0.986$); larger association rate constants occur with ligands that also have larger dissociation rate constants. This is consistent with each ligand having a different height to an energy barrier between the bound and unbound states. A decrease in the barrier height while keeping the bound state at an unchanged energy, for example, would increase both k_r and k_f proportionately. The similar energy states for the LR_s complex for all ligands may be related to the observation that all six ligands were equal agonists[2] for all three responses. This suggests the hypothesis that ligand efficacy is dictated by the energy state of the ligand−receptor complex, whereas potency is at least in part dictated by the kinetics of ligand−receptor binding and processing. The parameters k_f and k_r were each highly correlated with K_{dx}, a point to which we will return below.

The receptor conversion rate constant, k_x, was found to be highly ligand dependent (varying over a 200-fold range, Table 1). The ligands affiliate in two groups based on the value of k_x, CHO-NLFNYK-FL, CHO-NLFNYK-TMR, and CHO-MLKKF-FL with $k_x \sim 10^{-2}$ s^{-1}; and CHO-VLFK-FL, CHO-MLF, and CHO-NLF with $k_x \sim 10^{-4}$ s^{-1}. The implication of this difference is that for CHO-NLFNYK-FL, CHO-NLFNYK-TMR, and CHO-MLFFK-FL, both affinity states (LR_s and LR_x) will be present at substantial magnitudes within tens of seconds after ligand binding is initiated, and after minutes of binding, the majority of the bound receptors will be in the LR_x state. For CHO-VLFK-FL, CHO-MLF, and CHO-NLF on the other hand, the initially formed LR_s persists for a longer time. For comparison, 1 h of binding of CHO-NLFNYK-FL at 4 °C produces ~98% bound receptors in the LR_x state, while only ~30% of the CHO-VLFK-FL bound receptors are in the LR_x state after 1 h of binding.

The forward rate constants for ligand binding to R_x (Table 1) were similar to those for R_s (on the order of 10^6 $M^{-1}s^{-1}$) for the fluorescently labeled ligands but 5 orders of magnitude less for the unlabeled ligands, indicating that the fluorescent label may have significantly increased the affinity of ligand for the R_x state. The values of k_{r2} varied over 2 orders of magnitude and the resulting calculated K_{dx} values varied 7000-fold.

Measurement of N-Formyl Peptide-Induced Responses.

Actin Polymerization Elicited by N-Formyl Peptide Stimulation. The ability of each of the six N-formyl peptide ligands

[2] For the purpose of this report, we will refer to the maximum ability of a ligand to induce a response as "agonism". The concentration dependence of the ligands (i.e., ED_{50}s) will be referred to as "potency".

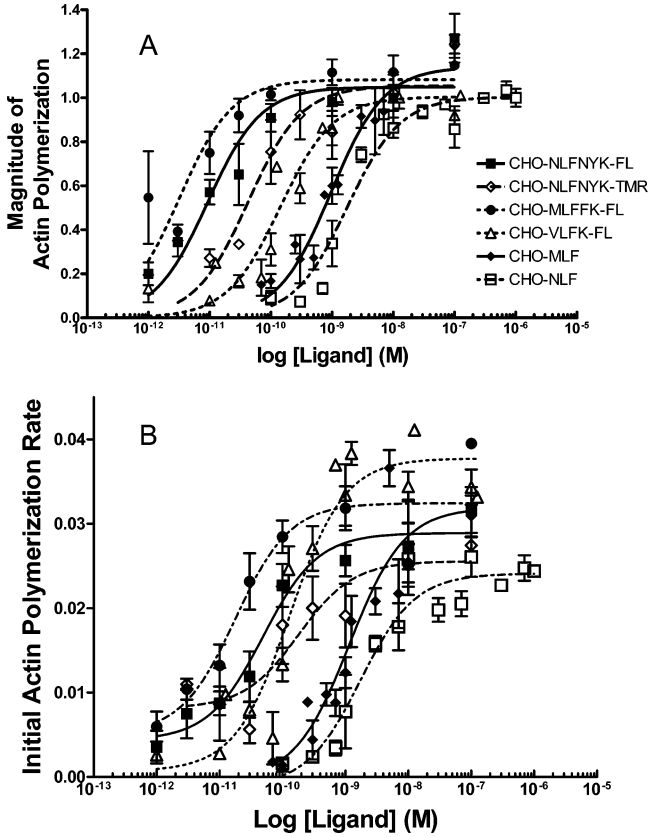

FIGURE 4: Magnitude and rate of actin polymerization versus ligand concentration. Dose response curves of actin polymerization were calculated from right angle light scatter data. The magnitude of the response was normalized to maximum response induced by CHO-NLFNYK-FL (A) and initial rate of actin polymerization was calculated from the first 5 s of the response and quantified as the fractional change per second (B). Error bars represent standard error of the mean: $n = 4$ for CHO-MLFFK-FL, CHO-NLFNYK-FL, and CHO-MLF; $n = 5$ for CHO-NLFNYK-TMR; and $n = 3$ for CHO-VLFFK-FL and CHO-NLF.

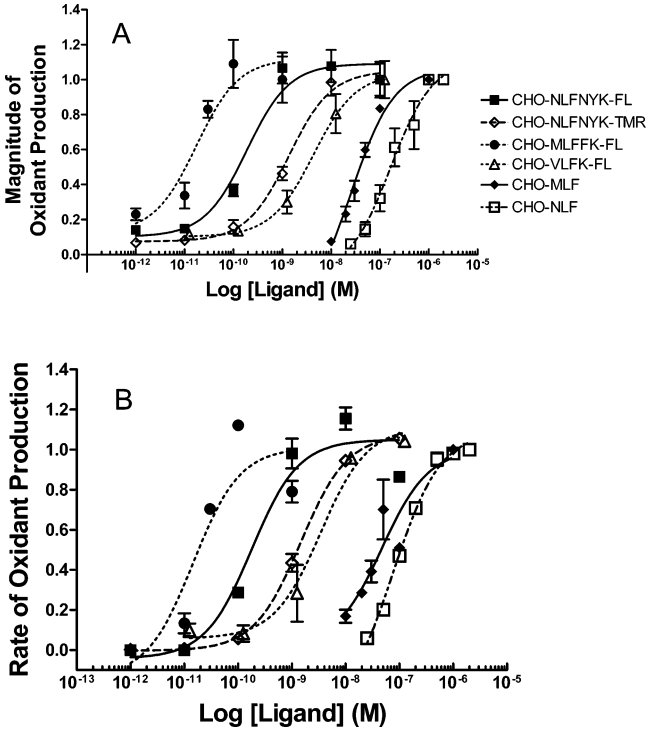

FIGURE 5: Magnitude and rate of oxidant production versus ligand concentration. The amount of oxidants produced 300 s post-stimulus (A) and the maximum rate of oxidant production (B) were normalized to the response level induced by a saturating concentration of CHO-NLFNYK-FL. Error bars represent standard error of the mean with $n = 2$ for CHO-NLFNYK-FL, CHO-NLFNYK-TMR, and CHO-MLFFK-FL; $n = 3$ for CHO-VLFK-FL and CHO-MLF; and $n = 4$ for CHO-NLF.

to produce a response was measured. Changes in right angle light scatter (RALS) have been shown to be inversely proportional to actin polymerization via pseudosimultaneous protocols (*26*, *27*). By monitoring actin polymerization via right angle light scattering at 340 nm, it was evident that all six of the ligands stimulated the characteristic biphasic response; actin polymerization reached a maximum around 10 s after ligand addition, and subsequently, the actin depolymerized over the next 3−5 min (*51*).

The magnitude of actin polymerization was normalized to the maximal response induced by CHO-NLFNYK-FL and the dose response curves for the six ligands plotted (Figure 4A). All of the ligands investigated yielded the same maximum value of RALS change, indicating that all of the ligands were equal agonists for eliciting actin polymerization. The concentrations that elicited half of the maximum actin polymerization response, ED_{50}, for the different ligands are listed in Table 1. The rank order of the potencies were as follows: CHO-MLFFK-FL > CHO-NLFNYK-FL > CHO-NLFNYK-TMR > CHO-VLFK-FL > CHO-MLF > CHO-NLF.

The data were also utilized for quantification of the maximum rate of actin polymerization as estimated by a linear fit through the initial data points (0−5 s) after ligand stimulation. The rates (fractional change per second) are plotted versus ligand concentration in Figure 4B. ED_{50} values for the rate of actin polymerization are included in Table 1, with the same rank order of potencies as magnitude of actin polymerization. The ED_{50} values determined from the actin polymerization rate and magnitude were highly correlated (Table 2, $r = 0.997$).

Oxidant Production Elicited by N-Formyl Peptide Stimulation. Compared with actin polymerization, the time scale of oxidant production was longer. After ligand addition, there was an increase in fluorescence, which corresponded with increased O_2^- that reached a plateau by three minutes. The maximum response for all ligands corresponded to ~ 11 nM $H_2O_2/5 \times 10^6$ cells, and thus all ligands investigated were equal agonists (Figure 5). Oxidant production was normalized to the maximum response induced by CHO-NLFNYK-FL, and the resulting dose response curve plotted (Figure 5A). The maximum rate of oxidant production was also calculated (using SLM-8100 software to calculate the first derivative of the data) and likewise normalized to the maximum rate of response induced by CHO-NLFNYK-FL and plotted (Figure 5B). The estimated ED_{50} values are listed in Table 1. The ED_{50} values determined from the rate and magnitude of oxidant production were correlated (Table 2, $r = 0.900$), and were of the same rank order as the rate and magnitude of actin polymerization.

Activation of G-Proteins by N-Formyl Peptides. Isolated plasma membranes were utilized to measure the abilities of N-formyl peptides to stimulate G-protein activity measured as enhanced binding of radiolabeled GTPγS. Maximum responses for all ligands were similar, indicating that the

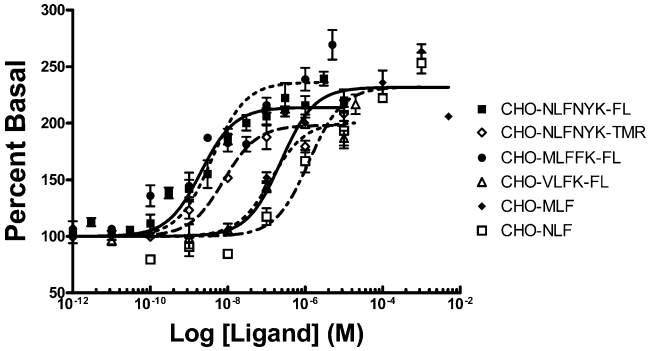

FIGURE 6: Dose−response curves for ligand-induced G-protein activation. [^{35}S]GTPγS binding to plasma membranes was measured (mean ± standard error of the mean) with varying concentrations of N-formyl peptides CHO-NLFNYK-FL ($n = 10$), CHO-NLFNYK-TMR ($n = 3$), CHO-MLFFK-FL ($n = 6$), CHO-VLFK-FL ($n = 4$), CHO-MLF ($n = 9$), and CHO-NLF ($n = 2$). The response was quantified as percent [^{35}S]GTPγS binding in the absence of ligand (percent basal).

degree of agonism is not highly dependent upon ligand structure even at this early step in the signal transduction cascade (Figure 6). The ED_{50}s for the [^{35}S]GTPγS binding responses were of rank-order similar to that of the actin and oxidant responses: CHO-NLFNYK-FL ≈ CHO-MLFFK-FL > CHO-NLFNYK-TMR > CHO-VLFK-FL ≈ CHO-MLF > CHO-NLF (Table 1). It is notable that the ED_{50}s for the [^{35}S]GTPγS binding assay were 2−3 orders of magnitude greater than the corresponding ED_{50}s for the actin and oxidant assays, suggesting that post-receptor events contribute amplification to responses. Alternatively, assays of responses in membranes and intact cells may not be directly comparable. This lower sensitivity of G-protein activation assays compared to whole cell response assays has been noted for other GPCR systems (*52*).

Interrelationships Among Responses Induced by N-Formyl Peptides. All six N-formyl peptides were equal agonists for the actin and oxidant responses and G-protein activation (Figures 4−6). The ED_{50} values for the responses (Table 1) varied among the ligands, with the ED_{50} rank order of G-protein activation, actin polymerization, and oxidant production correlating highly with each other (Table 2; r ranges from 0.908 to 0.997). If a ligand was better at stimulating one response, it was also better at stimulating the other responses. This correlation was not one-to-one, however. Across the six ligands, the ED_{50} values for actin polymerization varied over 600-fold (2×10^{-9} M to 3×10^{-12} M), whereas the ED_{50} values for oxidant production varied over a 10 000-fold range (2×10^{-7}−2×10^{-11} M). For the most active ligands, the ED_{50} values of the two intact cell responses were similar (e.g., the ED_{50} values for both responses elicited by CHO-MLFFK-FL are approximately 10^{-11}M). However, for the least active ligand (CHO-NLF) the ED_{50} values for the two responses differed by 2 orders of magnitude. The greater sensitivity of the actin response compared to the oxidant response to CHO-NLFNYK-FL, and CHO-MLF has been previously noted (*29*, *53*−*55*).

The level of agonism and the rank order of potencies of ligands for the actin and oxidant responses were the same as for the [^{35}S]GTPγS binding assay, indicating the differences in abilities of ligands to mediate responses must be determined upstream of G-protein activation (i.e., at the level of ligand−receptor interactions).

Is The Binding Model Able to Explain Response Potency? The correlation matrix of Table 2 indicates the response ED_{50} values are positively correlated with the binding parameters k_f, k_r, and K_{dx}. It is intuitively reasonable that k_r and ED_{50} values would be positively correlated, given that LR_s is the signaling receptor state; the larger k_r, the shorter the lifetime of the LR_s complex, and the greater the amount of ligand that would be needed to maintain stimulatory levels of LR_s complexes. In contrast, a positive correlation between k_f and response ED_{50} values is not as easily rationalized; the higher k_f, the faster LR_s would be generated, and one would expect this to decrease the amount of ligand needed to produce half-maximal response. However, k_f and k_r are not independent parameters but are themselves highly correlated (as previously noted). Given that k_r varies over a greater range than k_f, its effect on responses appears to dominate. The parameters k_f and k_r were each highly correlated with K_{dx}, although the reason behind this correlation is not obvious. However, we note that a correlation matrix evaluates pairs of parameters for linear relationships and would not detect the presence of nonlinear relationships or interactions of parameters[3].

The above statistical analyses were limited in that they assessed only linear relationships between parameters and assumed parameters were independent. Given the observation that k_f and k_r correlated with each other and with K_{dx}, complex interactions of parameters could not be deciphered by these simple statistical tests. Thus, a more rigorous test of the ability of Scheme 1 to predict responses was designed. It was assumed that if LR_s is the signaling receptor state, then responses should be related to the formation of LR_s. Thus, the binding parameters of Table 1 were utilized to simulate formation of LR_s for each experimental condition of ligand and concentration as described in Methods. Response data were then plotted versus the rate of formation of LR_s or the integrated amount of LR_s for each condition of ligand type and concentration to generate dose−response curves. Figure 7 depicts representative results for magnitude of oxidant production and magnitude of actin polymerization versus integrated LR_s. If responses were directly related to the formation of LR_s, we would expect all the curves of Figure 7 to coincide; however, the curves are still separated by orders of magnitude differences in integrated LR_s values similar to what is seen in plots of responses versus ligand concentration (Figures 4−6). The same observation was made from plots of response rates versus rate of formation of LR_s, rate of formation of LR_x, or integrated amount of LR_x (data not shown, *51*). Thus, calculated values of either LR_s or LR_x do not adequately account for response behavior. This result suggests that whereas the interconverting two-receptor state model of Scheme 1 is adequate to describe

[3] Multiple regression analysis was utilized to assess the possibility of parameter interactions. This analysis determines the ability of the data to be fit as a linear combination of independent variables. However, all parameters could not be evaluated simultaneously because the analysis requires there be more "subjects" (in our case, six ligands) than the number of variables (in our case, 12). In addition, independence of variables is assumed, but in our case, several variables were correlated. Thus, multiple regression analyses were performed to determine the effect on one response at a time of various combinations of up to four uncorrelated parameters at a time. In agreement with the correlation matrix, these analyses identified k_f, k_r, and K_{dx} as important contributors to responses, but showed no additional relationships.

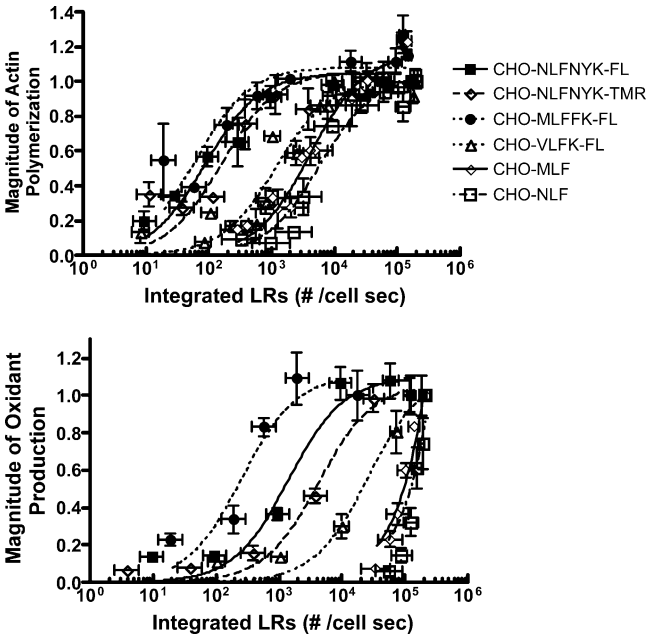

FIGURE 7: Magnitude of oxidant production and actin polymerization versus integrated number of signaling complexes, LR_s. Response data of Figures 4A and 5A are plotted versus integrated LR_s for each ligand condition as described in Methods. Error bars for LR_s were estimated for high LR_s and low LR_s scenarios as described in Methods.

the binding behavior, it is inadequate to account for response data.

DISCUSSION

Our aim in this study was to elucidate the relationships between receptor states and cellular responses in the N-formyl peptide receptor system on the neutrophil as a model of a GPCR system in a physiologically relevant context. This is the first rigorous test of how well a kinetic binding model works to predict response data for a group of ligands that bind to the same receptor. The level of agonism and the rank order of potencies of ligands for the actin and oxidant responses were the same as that for the [^{35}S]GTPγS binding assay, indicating that differences in abilities of ligands to mediate responses must be determined upstream of G-protein activation (i.e., at the level of ligand−receptor interactions). Thus, we compared binding rate constants and response characteristics to understand how ligand binding parameters dictate response characteristics.

The binding of CHO-MLFFK-FL and CHO-VLFK-FL at 4 °C, like the previously studied ligands CHO-NLFNYK-FL, CHO-NLFNYK-TMR, CHO-MLF, and CHO-NLF, were best fit by the interconverting two-site binding model given in Scheme 1, confirming the general applicability of the model for describing binding of this class of compounds to the N-formyl peptide receptor. LR_x is thought to be a nonsignaling receptor state because a high affinity ligand−receptor complex persists on the cell surface well after responses have terminated (*29*). Whereas the presence of a lower affinity receptor state correlates with the ability of a ligand to induce responses, the formation of a higher affinity receptor state correlates with desensitization of responses (*35*). Thus, LR_s and LR_x appear to be signaling and nonsignaling receptor states, respectively.

The Relationship Between LR_s and Responses. Our observations that k_f and k_r, rate constants that influence the levels of LR_s, correlate with responses supports the evidence that LR_s is the signaling receptor state. However, the response ED_{50} values across all ligands varied over 100−10,000-fold, whereas the values for the rate constants k_f and k_r varied less than 50-fold, indicating that there is not a simple relationship between the response characteristics and the forward and reverse rate constants for binding to the R_s state. Thus, we attempted to relate the ED_{50}s of responses with the calculated number or rates of formation of LR_s complexes using Scheme 1 and taking into account the combined effects of k_f, k_r, and k_x on LR_s formation; this approach did not satisfactorily explain our observations for these six ligands, even if changes in the rate constants with temperature were taken into account (Figure 7) (*51*).

An additional example of the lack of Scheme 1 to account for response data can be seen by examining the values of the receptor interconversion rate constant k_x that dictates removal of receptors from the presumed signaling state (R_s) to the presumed nonsignaling state (R_x) and as such is expected to contribute to ligand potency. One might expect if LR_s is the signaling state of the receptor that a slower rate of depletion of LR_s (by conversion to the LR_x state) would coincide with a more active ligand. However, this was not seen: the least active ligands fell into the class with slower conversion rate constants.

Thus, while Scheme 1 describes the ligand binding behavior well, it is insufficient to predict response potency. It is notable that the ratios of k_r/k_f, the calculated K_{ds} for the lower affinity receptor state, are very similar for the six ligands studied. This observation suggests that the LR_s state for all ligands are of similar energy level, and we hypothesize that the similar energy level of the LR_s state and the similar agonism of the ligands are related. This is consistent with the hypothesis that GPCRs can exist in many conformational states with differing probabilities, representing an "energy landscape" or "receptor ensemble" (*57*, *58*) and with data that full agonists for GPCRs drive the receptor into the same conformational state, whereas partial agonists drive the receptor into alternative conformational states (*4*, *16*, *17*). In the context of the N-formyl peptide receptor, full agonism may be related to the fact that all six ligands studied are N-formyl peptides. Partial agonists that do not have N-formyl groups have been identified for the N-formyl peptide receptor (*61*); these partial agonists may prove useful in assessing the relationship between efficacy and the energy level of the LR_s state.

The Nature of LR_x. As noted above, LR_x, the high affinity receptor state, has previously been interpreted as an inactive receptor state. Phosphorylation and binding of arrestin to GPCRs is known to increase receptor affinity for ligand (*7*, *11*). Whether or not LR_x measured for the N-formyl peptide receptor at 4 °C is a phosphorylated, arrestin-bound state is not known. However, it is questionable that significant phosphorylation could occur at 4 °C, the temperature of the binding studies in which conversion of the receptor to the LR_x state can be rather rapid ($k_x \sim 10^{-2}$/sec). Perhaps k_x represents a process involving a conformational change of the receptor that renders it accessible for subsequent phosphorylation reactions. Thus, LR_x detected with binding measurements may not be the same

as the high affinity desensitized receptor state detected by other methods.

The strong correlation of response ED_{50} values with K_{dx} prompted a reevaluation of the assumption that LR_x is a nonsignaling form of the receptor. The range of K_{dx} values over all ligands was 7000-fold, similar to the range of ED_{50} values for the oxidant response, and there was a strong correlation between response ED_{50} values and K_{dx} values (Table 2, $r = 0.879-0.999$), suggesting that response potency could be determined by the energy level of the LR_x complex. The observation that the least active ligands were the slowest to convert LR_s to LR_x further supports the hypothesis that LR_x may play a role in signaling. However, we note that the formation of LR_x is highly dependent on conversion from the LR_s state; since dissociation of ligand from LR_x is relatively slow, little re-binding of L to R_x occurs. Thus the formation of LR_x is a relevant parameter to track. However, attempts to correlate the ED_{50} values of responses and the calculated rates of formation or integrated values of the LR_x complex (again using Scheme 1 and taking into account the combined effects of k_{f2}, k_{r2}, and k_x on LR_x formation) did not explain the differences in the ED_{50} values for the six ligands even if changes in the rate constants with temperature were taken into account (data not shown, *51*). Nonetheless, K_{dx} was highly correlated with k_f and k_r, suggesting relationships between the receptor states that have not yet been identified. Taken together, these analyses indicate that while Scheme 1 describes the ligand binding behavior well and suggests a physical basis for the concept of ligand efficacy, it is insufficient to predict response potency.

Predicting Response Potency. One possibility to explain the insufficiency of the model in Scheme 1 to predict response behavior is that there may be receptor states not discriminated by the model. Binding models—such as that presented in Scheme 1—reflect only the receptor states that are necessary to describe the binding data. There may in fact be additional receptor states present, but they would not be detected if the number of receptors in these additional states is small and/or if the binding kinetics are quite similar to those of other receptor states (*59*, *60*). In these cases, inclusion of these additional states in the model would not improve the goodness of fit to the binding data, and therefore their inclusion would not be justified in the development of a binding model. This possibility is consistent with studies that show occupancy of relatively few receptors are required to initiate responses; occupancy of as few as 10% of N-formylpeptide receptors by CHO-NLFNYK-FL is sufficient to induce half-optimal rate of oxidant production, and 10−20 occupied receptors are sufficient to induce half-optimal actin polymerization response (29).

In fact, additional receptor states for GPCRs have been suggested. Active and inactive states of the receptor have been found to be useful to adequately account for constitutively active mutant receptors and the action of inverse agonists in the β-adrenergic receptor system (*2*, *3*, *58*), and have been suggested by mutant receptor studies in the N-formyl peptide receptor system (*5*). It is worth pointing out, however, that these additional receptor states have been incorporated into equilibrium models, while in our case, we focus on the more physiologically relevant unsteady-state dynamics that are inherent in GPCR signaling. In the context of the present work, then, one might consider models containing two or more LR_s states with differing abilities to activate G-proteins and be converted to the LR_x form. Discrimination of these receptor states will rely upon a combination of binding and response data: the data presented here provide a reference point for these future studies and demonstrate the need to test these possibilities.

APPENDIX

The analysis of data for CHO-VLFK-FL binding predicted that within the 3−5 min in which dissociation data was collected, little conversion from low- to high-affinity states would have occurred. Thus, an alternative method for analyzing the kinetic binding data of CHO-VLFK-FL was used to validate the values of k_r and k_x evaluated by the full model fit. Long-time dissociation data were utilized for this analysis. The following assumptions were made for this alternative data analysis. During the time course of the long-time dissociation data collection (3−5 min) there was insignificant conversion of LR_s to LR_x. In other words, the dissociation data could be analyzed as two independent receptor states. The second assumption was that the dissociation from the high-affinity state (LR_x) was relatively slow (estimates from analysis yielded values of $k_{r2} \sim 10^{-3}$ s^{-1}). Therefore, all of the ligand dissociation monitored over the 3−5 min period was attributable to the LR_s state of the receptor, and LR_x would appear as a nondissociating receptor state. Thus, the long-time dissociation data could be fit with a single-site model expressed as a single-phase exponential decay with a plateau as a function of time (t)

$$LR_{app} = LR_s \exp(-Kt) + LR_x \qquad (2)$$

where LR_s is the difference between LR_{app} measured and LR_x where the data plateaus, and K is the decay exponent. As with other data analysis, LR_{app} is the sum of LR_x and LR_s. Due to the assumption that only LR_s dissociation was monitored, K was assumed to be equal to k_r.

Thus, by fitting long-time dissociation data of CHO-VLFK-FL to a single phase exponential decay function, values of k_r, LR_s and LR_x were obtained. By varying the amount of time cells were incubated with CHO-VLFK-FL before initiating dissociation, values of LR_s and LR_x at varying times could be measured. These data for LR_s and LR_x as a function of time were utilized to calculate the conversion rate constant, k_x, as they applied to the following model:

Scheme 2

$$LR_s \xrightarrow{k_x} LR_x$$

Thus, a plot (LR_x/LR_s) versus time yielded a line with slope of k_x.

The data are depicted in Figure 8. Panel A shows a single-exponential decay fit to a dissociation curve, from which k_r was calculated using Equation 2. Panel B shows the ratio of LR_x/LR_s at various times after initiating ligand binding; the slope of this line equals k_x. As a result of this alternative data analysis, a value for k_r of $2.4 \pm 0.8 \times 10^{-2}$ s^{-1} was calculated, and this value was within 3-fold of the value evaluated by fitting the data to the full interconverting two-site model ($7.8 \pm 2.0 \times 10^{-2}$ s^{-1}). The value of k_x calculated

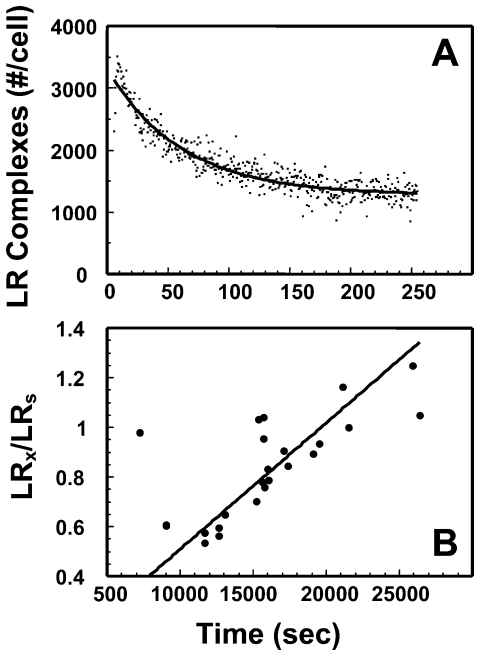

FIGURE 8: Kinetic data analysis for CHO-VLFK-FL. (A) Long-time dissociation data of 3 nM CHO-VLFK-FL (dots) were fit with a single-phase exponential decay (line). (B) LR complex ratio LR_x/LR_s (dots) graphed versus time and fit to a line to evaluate k_x for CHO-VLFK-FL ($n = 6$).

from this alternative method was $2.7 \pm 0.6 \times 10^{-5}$ s^{-1}, and was within 7-fold of the value evaluated by fitting the data to the full interconverting two-site model ($1.80 \pm 0.7 \times 10^{-4}$ s^{-1}). Thus, the two methods of data analysis agreed well.

ACKNOWLEDGMENT

We thank Mary J. Clark for assistance with the [^{35}S]GTPγS binding measurements.

REFERENCES

1. Gether, U. (2000) Uncovering molecular mechanisms involved in activation of G protein-coupled receptors, *Endocrine Rev. 21*, 90−113.
2. Weiss, J. M., Morgan, P. H., Lutz, M. W., and Kenakin, T. P. (1996) The cubic ternary complex receptor-occupancy model. I. Model description, *J. Theor. Biol. 178*, 151−167.
3. Samama, P., Cotecchia, S., Costa, T., and Lefkowitz, R. J. (1993) A mutation-induced activated state of the β_2-adrenergic receptor: extending the ternary complex model, *J. Biol. Chem. 268*, 4625−4636.
4. Gether, U., Lin, S., and Kobilka, B. K., (1995) Flourescent labeling of purified β_2 adrenergic receptor: Evidence for ligand-specific conformational changes, *J. Biol. Chem. 270*, 28268−28275.
5. Prossnitz, E. R., Gilbert, T. L., Chaing, S., Campbell, J. J., Qin, S., Newman, W., Sklar, L. A., and Ye, R. D. (1999) Multiple activation steps of the N-formyl peptide receptor, *Biochemistry 38*, 2240−2247.
6. Bennett, T. A., Foutz, T. D., Gurevich, V. V., Sklar, L. A., and Prossnitz, E. R. (2001) Partial phoshorylation of the N-formyl peptide receptor inhibits G protein association independent of arrestin binding, *J. Biol. Chem. 276*, 49195−49203.
7. Gurevich, V. V., Pals-Rylaarsdam, R., Benovic, J. L., Hosey, M. M., and Onorato, J. J. (1997) Agonist-receptor-arrestin, an alternative ternary complex with high agonist affinity, *J. Biol. Chem. 272*, 28849−28852.
8. Luttrell, L. M. and Lefkowitz, R. J. (2002) The role of β-arrestins in the termination and transduction of G-protein-coupled receptor signals, *J. Cell Sci. 115*, 455−465.
9. Miller, W. E. and Lefkowitz, R. J. (2001) Expanding roles for β-arrestins as scaffolds and adaptors in GPCR signaling and trafficking, *Curr. Opin. Cell Biol. 13*, 139−145.
10. Kohout, T. A. and Lefkowitz, R. J. (2003) Regulation of G protein-coupled receptor kinases and arrestins during receptor desensitization, *Mol. Pharmacol. 63*, 9−18.
11. Key, T. A., Bennett, T. A., Foutz, T. D., Gurevich, V. V., Sklar, L. A., and Prossnitz, E. R. (2001) Regulation of formyl peptide receptor agonist affinity by reconstitution with arrestins and heterotrimeric G-proteins, *J. Biol. Chem. 276*, 49204−49212.
12. Koenig, J. A. and Edwardson, J. M. (1997) Endocytosis and recycling of G protein-coupled receptors, *Trends Pharmacol. Sci. 18*, 176−287.
13. Lefkowitz, R. J. (1998) G Protein-coupled receptors: New roles for receptor kinases and β-arrestins in receptor signaling and desensitization. *J. Biol. Chem. 273*, 18677−18680.
14. Sklar, L. A., Finney, D. A., Oades, Z. G., Jesaitis, A. J., Painter, R. G., and Cochrane, C. G. (1984) The dynamics of ligand−receptor interactions: Real-time analysis of association, dissociation, and internalization of an N-formly peptide and its receptors on the human neutrophil, *J. Biol. Chem. 259*, 5661−5669.
15. Zigmond, S. H., Sullivan, S. J., and Lauffenburger, D. A. (1982) Kinetic analysis of chemotactic peptide receptor modulation, *J. Cell Biol. 92*, 34−43.
16. Kobilka, B. K. (2002) Agonist-induced conformational changes in the β_2 adrenergic receptor, *J. Peptide Res. 60*, 317−321.
17. Salamon, Z., Hruby, V. J., Tollin, G., and Cowell, S. (2002) Binding of agonists, antagonists, and inverse agonists to the human δ-opioid receptor produces distinctly different conformational states distinguishable by plasmon-wavequide resonance spectroscopy, *J. Peptide Res. 60*, 322−328.
18. Singh, V. K., Bajpai, K., Biswas, S., Haq, W., Khan, M. Y., and Mathur, K. B. (1997) Molecular biology of opioid receptors: recent advances, *Neuroimmunomodulation 4*, 285−297.
19. Milligan, G., MacEwan, D. J., Mercouris, M., and Mullaney, I. (1997) Inverse agonism at adrenergic and opioid receptors: studies with wild type and constitutively active mutant receptors, *Receptors and Channels 5*, 209−213.
20. Prossnitz, E. R. and Ye, R. D. (1997) The N-formyl peptide receptor: a model for the study of chemoattractant structure and function, *Pharmacol. Therapeut. 74*, 73−102.
21. Sklar, L. A. (1987) Real-time spectroscopic analysis of ligand−receptor dynamics, *Annu. Rev. Biophys. Biophys. Chem. 16*, 479−506.
22. Hoffman, J. F., Linderman, J. J., and Omann, G. M. (1996) Receptor upregulation, internalization, and interconverting receptor states: critical components of a quantitative description of N-formylpeptide-receptor dynamics in the neutrophil, *J. Biol. Chem. 271*, 18394−18404.
23. Hoffman, J. F., Keil, M. L., Riccobene, T. A., Omann, G. M., and Linderman, J. J. (1996) Interconverting receptor states at 4 °C for the neutrophil N-formyl peptide receptor, *Biochemistry 35*, 13047−13055.
24. Waller, A, Pipkorn, D., Sutton, K., Linderman, J. J., and Omann, G. M. (2001) Validation of flow cytometric competitive binding protocols and characterization of fluorescently labeled ligands, *Cytometry 45*, 102−114.
25. Omann, G. M. and Sklar, L. A. (1989) Spectrofluorometric analyses of cell responses: Activation of neutrophils by chemoattractants and hexachlorocyclohexanes, in *Luminescence Applications in Biological, Chemical, Environmental, and Hydrological Sciences* (Goldberg, M. C., Ed.) pp 23−44, ACS Publications, Washington, DC.
26. Omann, G. M., Oades, Z. G., and Sklar, L. A. (1985) Simultaneous spectrofluorometric analysis of cell responses, *Biotechniques 3*, 508−512.
27. Sklar, L. A., Omann, G. M., and Painter, R. J. (1985) Relationship of actin polymerization and depolymerization to light scattering in human neutrophils. Dependence on receptor occupancy and intracellular calcium, *J. Cell Biol. 101*, 1161−1166.
28. Hyslop, P. A., and Sklar, L. A. (1984) A quantitative fluorometric assay for the determination of oxidant production by polymorphonuclear leukocytes: Its use in the simultaneous fluorometric assay of cellular activation processes, *Anal. Biochem. 141*, 280−286.
29. Sklar, L. A., Hyslop, P. A., Oades, Z. G., Omann, G. M., Jesaitis, A. J., Painter, R. G., and Cochrane, C. G. (1985) Signal transduction and ligand−receptor dynamics in the human neutrophil. Transient responses and occupancy-response relations at the formyl peptide receptor, *J. Biol. Chem. 260*, 11461−11467.
30. Linderman, J. J. (2000) Kinetic modeling approaches to understanding ligand efficacy, in *The Pharmacology of Functional, Biochemical, and Recombinant Receptor Systems*, *Handbook of*

Experimental Pharmacology Volume 148, (Kenakin, T and Angus, A., Eds.) pp 119−146, Springer-Verlag, Secaucus, NJ.
31. Vilven, J. C., Domalewski, M., Prossnitz, E. R., Ye, R. D., Muthukumaraswamy, N., Harris, R. B., Freer, R. J., and Sklar. L. A. (1998) Strategies for positioning fluorescent probes and cross-linkers on formyl peptide ligands, *J. Rec. Sig. Trans. Res. 18*, 187−221.
32. Freer, R. J., Day, A. R., Muthukumaraswamy, N., Pinon, D., Wu, A., Showell, H. J., and Becker, E. L. (1982) Formyl peptide chemoattractants: a model of the receptor on rabbit neutrophils, *Biochemistry 21*, 257−263.
33. Rot, A., Henderson, L. E., Copeland, T. D., and Leonard, E. J. (1987) A series of six ligands for the human formyl peptide receptor: tetrapeptides with high chemotactic potency and efficacy, *Proc. Natl. Acad. Sci. U.S.A. 84*, 7967−7971.
34. Sklar, L. A., Mueller, H., Omann, G. M., and Oades, Z. G. (1989) Three states for the formyl peptide receptor on intact cells, *J. Biol. Chem. 264*, 8483−8486.
35. Jesaitis, A. J., Tolley, J. O. and Allen, R. A. (1986) Receptor-cytoskeleton interactions and membrane traffic may regulate chemoattractant-induced superoxide production in human granulocytes, *J. Biol. Chem. 261*, 13662−13669.
36. Fay, S. P., Domalewski, M. D., and Sklar, L. A. (1993) Evidence for protonation in the human neutrophil formyl peptide receptor binding pocket, *Biochemistry 32*, 1627−31.
37. Kermode, J. C., Freer, R. J., and Becker, E. L. (1991) The significance of functional receptor heterogeneity in the biological responses of the rabbit neutrophil to stimulation by chemotactic formyl peptides, *Biochem. J. 276*, 715−723.
38. Tolley, J. O., Omann, G. M., and Jesaitis, A. J. (1987) A high yield, high-purity elutriation method for preparing human granulocytes demonstrating enhanced experimental lifetimes, *J. Leuk. Biol. 42*, 43−50.
39. Suchard, S. J. and Mansfield, P. J. (1996) Neutrophil thrombospondin receptors are linked to GTP-binding proteins, *J. Cell. Physiol. 168*, 217−227.
40. Bradford, M. M. (1976) Rapid and sensitive method for quantification of microgram quantities of protein uoliing preic of protein-dye binding, *Anal. Biochem. 72*, 248−254.
41. Sklar, L. A., Oades, Z. G., and Finney, D. A. (1984) Neutrophil degranulation detected by right angle light scattering: spectroscopic methods suitable for simultaneous analyses of degranulation or shape change, elastase release, and cell aggregation, *J. Immunol. 133*, 1483−1487.
42. Sklar, L. A., Oades, Z. G., Jesaitis, A. J., Painter, R. G., and Cochrane, C. G. (1981) Fluoresceinated chemotactic peptide and high-affinity antifluorescein antibody as a probe of the temporal characteristics of neutrophil stimulation, *Proc. Natl. Acad. Sci. U.S.A. 78*, 7540−7544.
43. Sklar, L. A., and Finney, D. A. (1982) Analysis of ligand−receptor interactions with the fluorescence activated cell sorter, *Cytometry 3*, 161−165.
44. Clark, M. J., Harrison, C., Zhong, H., Neubig, R. R., and Traynor, J. R. (2003) Endogenous RGS protein action modulates μ-opioid signaling through $G_{\alpha o}$: Effects on adenylyl cyclase, extracellular signal-regulated kinases, and intracellular calcium pathways, *J. Biol. Chem. 278*, 9418−9425.
45. Ye, R. D. and Boulay, F. (1997) Structure and function of leukocyte chemoattractant receptors, *Adv. Pharmacol. 39*, 221−289.
46. Fiore, S., Maddox, J. F., Perez, H. D., and Serhan, C. N. (1994) Identification of a human cDNA encoding a functional high affinity lipoxin A_4 receptor, *J. Exp. Med. 180*, 253−260.
47. Fiore, S., Ryeom, S. W., Weller, P. F., and Serhan, C. N. (1992) Lipoxin recognition sites. Specific binding of labeled lipoxin A_4 with human neutrophils, *J. Biol. Chem. 267*, 16168−16176.
48. Fiore, S., and Serhan, C. N. (1995) Lipoxin A_4 receptor activation is distinct from that of the formyl peptide receptor in myeloid cells: inhibition of CD11/18 expression by lipoxin A_4-lipoxin A_4 receptor interaction, *Biochemistry 34*, 16678−16686.
49. Quehenberger, O, Prossnitz, E. R., Cavanagh, S. L., Cochrane, C. G., and Ye, R. D. (1993) Multiple domains of the N-formyl peptide receptor are required for high affinity ligand binding. Construction and analysis of chimeric N-formyl peptide receptors, *J. Biol. Chem. 268*, 18167−18175.
50. Christophe, T., Karlsson, A., Dugave, C., Rabiet, M.-J., Boulay, F., and Dahlgren, C. (2001) The synthetic peptide Trp-Lys-Tyr-Met-Val-Met-NH_2 specifically activates neutrophils through FPRL1/Lipoxin A_4 receptors and is an agonist for the orphan monocyte-expressed chemoattractant receptor FPRL2, *J. Biol. Chem. 276*, 21585−21593.
51. Waller, A. (2001) *Ligand binding and ligand efficacy in the N-formyl peptide receptor system on the human neutrophil.* Ph.D. Thesis, University of Michigan, Ann Arbor.
52. Umland, S. P., Wan, Y., Shah, H., Billah, M., Egan, R. W., Hey, J. A. (2000) Receptor reserve analysis of the human α_{2C}-adrenoreceptor using [^{35}S]GTPγS and camp functional assays, *Eur. J. Pharmacol. 411*, 211−221.
53. Omann, G. M., and Sklar, L. A. (1988) Response of neutrophils to stimulus infusion: differential sensitivity of cytoskeletal activation and oxidant production, *J. Cell Biol. 107*, 951−958.
54. Riccobene, T. A., Waller, A., Hoffman, J. F., Linderman, J. J., and Omann, G. M. (1998) Threshold and graded response behavior in human neutrophils: effect of varying G-protein or ligand concentrations, *Biochemistry 37*, 11534−11543.
55. Sklar, L. A. (1986) Ligand−receptor dynamics and signal amplification in the neutrophil, *Adv. Immunol. 39*, 95−143.
56. Sklar, L. A., Bokoch, G. M., Button, D., and Smolen, J. E. (1987) Regulation of ligand−receptor dynamics by guanine nucleotides: Real-time analysis of interconverting states for the neutrophil formyl peptide receptor, *J. Biol. Chem. 262*, 135−139.
57. Kenakin, T. (2003) Ligand-selective receptor conformations revisited: the promise and the problem, *Trends Pharmacol. Sci. 24*, 346−354.
58. Kenakin, T. (2002) Drug efficacy at G-protein-coupled receptors, *Annu. Rev. Pharmacol. Toxicol. 42*, 349−379.
59. Lauffenburger, D. A. and Linderman, J. J. (1993) *Receptors: Models for Binding, Trafficking, and Signaling*. Oxford University Press. New York, N. Y.
60. Munson, P. J. and Rodbard, D. (1980) Ligand: A versatile computerized approach for characterization of ligand-binding systems, *Anal. Biochem. 107*, 220−239.
61. Dalpiaz, A., Scatturin, A., Vertuani, G., Pecoraro, R., Borea, P. A., Varani, K., Traniello, S., Spisani, S. (2001) Met-Ile-Phe-Leu derivatives: full and partial agonists of human neutrophil formyl-peptide receptors, *Eur. J. Pharmacol. 411*, 27−33.

BI035335I